


Contents

Table of Contents	i
List of Figures	i
List of Tables	iii
1 Coupling NDs	1
1.1 Additional Experimental Methods	2
1.1.1 Nanomanipulator	2
1.1.2 Determination of The Position of Nanodiamonds	3
1.1.3 The Pick-And-Place Process	4
1.2 VCSELs	5
1.2.1 Vertical-Cavity Surface Emitting Laser Structure	6
1.2.2 SiV center in a Vertical-Cavity Surface Emitting Laser	7
1.3 Antennas	11
1.3.1 Plasmonic Antennas	13
1.3.2 Structure of the Plasmonic Antennas	15
1.3.3 SiV center in a Plasmonic Double Bowtie Antenna	16
Bibliography	21

List of Figures

1.1	(a) Sketch of the pick-and-place process exploiting a nanomanipulator. (b) Image of the nanomanipulator mounted in the FIB. The arrows indicate the degrees of freedom of motion of the nanomanipulator. The custom made workbench is situated in the middle of the picture. On top of it, there is a 1 cm^2 substrate with coated nanodiamonds, the nanomanipulator tip pointing to the middle of it. Behind it, there is the target vertical-cavity surface emitting laser. Perpendicular to the workbench, the objective of the electron microscope can be seen. The pointier cone perpendicular to the image top image edge is the objective of the focussed ion beam.	3
1.2	(a) Overview of a field of cross markers. The field spans $0.5 \times 0.5\text{ mm}$ (b) White light scan of an area with a cross marker in all four corners.	4
1.3	5
1.4	(a) Sketch of the VCSEL showing the different layers. ask how to cite (b) Image of the VCSEL. The circle with the black dots is the hole in the p-contact (diameter D_S , the smaller darker area in the middle is the laser output area (diameter D_A)	6
1.5	(a) Emission spectrum of the used VCSEL at two different currents. (b) Optical output power and voltage of the same VCSEL in dependence of input current. []	6
1.6	(a) SEM image of an array of VCSELs. The three wires are the anodes, which are connected to the top layer (p-contact) of the VCSEL. Therefore, three of the VCSEL structures can be operated. (b) Detail SEM image of the top of the exploited VCSEL Bm4. The circular middle part is the hole in the p-contact through which the top DBR is visible. The active diameter is smaller than that and not visible in the SEM.	7
1.7	(a) Scan of the VCSEL Bm4 with coupled nanodiamond under excitation with the laser from the confocal setup. The big visible ring is the edge of the circular hole in the p-contact. The bright spot in the upper left corner corresponds to the transferred nanodiamond containing an SiV center. (b) Scan of the VCSEL Bm2 without nanodiamond under excitation with the laser from the confocal setup. The circular hole in the p-contact exhibits a constant countrate.	8
1.8	(a) Spectrum of the preselected diamond for transfer onto VCSEL Bm4 before pick-and-place. The strong line denoted A exhibits a center wavelength of 746.0 nm and a linewidth of 1.9 nm . Line B exhibits a center wavelength of 0 nm and a linewidth of 0 nm put in correct numbers	

	(b) Spectrum of the same SiV center after pick-and-place, excited with the same laser as before. While Line A is almost gone, line B still exists and ist the predominant line of the spectrum. Note: different longpass filters were used for the two measurements. Measurement (a) was performed with a 720 nm longpass filter, measurement (b) with a 710 nm longpass filter.	8
1.9	(a) Scan of the laser light stemming from the VCSEL Bm4 and the fluorescence light light from the SiV center in the filter window 730 nm to 750 nm. (b) Scan of the laser light stemming from the VCSEL Bm2 without coupled SiV center. The outcome of the two scans is almost identical.	9
1.10	(a) Recorded Spectrum of the SiV center in the transferred nanodiamond on VCSEL Bm4 during VCSEL operation. No distinct SiV center lines are visible. (b) Recorded spectrum of VCSEL Bm2 (without SiV center)	9
1.11	Reflectivity of the Distributed Bragg reflector (DBR) of the VCSEL, and spectrum of the SiV center measured during VCSEL excitation. The reflectivity of the DBR and the VCSEL emission spectra are depicted with different scales. The shape of the measurement of the SiV center during VCSEL operation coincides with the shape of the DBR reflectivity. The spectrum of the SiV center is not visible. As the emission from the SiV center is small compared to the intensity of the laser sideband in the same wavelength regime, the SiV centers emission is not detectable warum schaut das spectrum anders aus als das, was einzeln geplottet ist?	10
1.12	(a) Picture recorded with a commercial high resolution laser scanning microscope. The area shaded in blue represents the photoluminescence scan in image (b). (b) Photoluminescence scan of a 8 $\mu\text{m} \times 13 \mu\text{m}$	11
1.13	<caption>	12
1.14	Image of the sample surface of 100 nm wet-milled nanodiamonds spin-coated on an iridium substrate illuminated with diffuse white light. The white bars are the horizontal bars of the cross markers which serve as a coarse orientation on the sample surface, the white dots are nanodiamonds, the big black spot is an artifact.	12
1.15	13
1.16	<caption>	15
1.17	15
1.18	<caption>	16
1.19	<caption>	18
1.20	<caption>	18
1.21	<caption>	18
1.22	<caption>	19
1.23	<caption>	19
1.24	<caption>	20

List of Tables

Chapter 1

Coupling Nanodiamonds to Photonic Structures

In the last chapter, we saw that the spectroscopic properties of SiV centers vary strongly among individual nanodiamonds. Nanodiamonds are further implemented in photonic structures for the application in metrology as well as in quantum cryptography or quantum computing. Therefore, it is important to have a good knowledge of the spectroscopic properties of the individual SiV center. A preselection of nanodiamonds including an SiV center with optimal properties is performed. These properties contain both spectroscopic parameters as well as technical parameters for the pick-and-place process. Spectroscopic parameters contain narrow linewidth, high countrates and single photon emission, the technical parameters include a size of the nanodiamonds hosting the SiV center bigger than 70 nm and how isolated they lie on the substrate surface. The selected nanodiamond is then transferred to a target structure. In the scope of this thesis, nanodiamonds including SiV centers were coupled to two different kinds of structures:

- Vertical-Cavity Surface Emitting Lasers: The aim is to create a hybrid-integrated single photon source, where an electric current is employed to create single photons. The diamond containing an SiV center is placed directly on the beam output. Hence the SiV center is directly pumped by the laser beam. As the SiV center emits in another wavelength regime than the pump laser, the single photons are accessible after filtering the VCSEL laser light. This single photon source is interesting for metrological applications, as it is the major building block for a portable device ready to calibrate single photon detectors.
- Plasmonic Nanoantennas: The aim is to enhance photoluminescence intensity. As described in previous chapters, not only ZPL position and linewidth, but also the photoluminescence intensity varies strongly among individual SiV centers. However, in metrology a photon flux rate high enough to be measured by a low optical flux detector is needed [1]. This increase in intensity is achieved by coupling the SiV centers in nanodiamonds to plasmonic antennas. Furthermore, plasmonic antennas can be used to tune the emitters' photoluminescence spectrum.

think
of other
word

1.1 Additional Experimental Methods

To couple nanodiamonds to photonic structures, we pursued several different methods:

1. Directly spin-coat the structures with a nanodiamond solution and consecutively look for a structure containing a nanodiamond with an SiV center exhibiting the desired spectroscopic properties. This method was tried with the antenna structures, as there are many antenna structures on one substrate (see Figure 1.13a), therefore there is a chance that a suited nanodiamond is incidentally ends up at the right spot. However, it is not suitable for the VCSELs, first because of the morphology of the VCSELs and secondly, because there is a very limited number of VCSELs on one substrate.
2. Use an iridium substrate covered with nanodiamonds containing SiV centers, look for a suited nanodiamond and transfer it with a pick-and-place technique using a nanomanipulator. The nanomanipulator is essentially a thin tip in a scanning electron microscopy. The iridium substrate is preprocessed with markers, to record the position of the preselected nanodiamond. The huge advantage is that the very best suited nanodiamond can be preselected. However, disadvantages of this process include the electron radiation during the pick-and-place process, which might affect SiV center fluorescence light and the further restriction that the nanodiamonds must be big enough to be picked up with the nanomanipulator.
3. Similar to method 2, however the transfer is performed with an atomic force microscope. While this method has the advantage that the nanodiamonds are not irradiated with electrons, the disadvantage is that it is not possible to observe the picking process in real time. The area of the preselected nanodiamond has to be scanned after every pick-up try, which is very time consuming and therefore was not further pursued after some trials.

In the following paragraphs, the pick-and-place technique of method 2 is described in more detail. It is the coupling method most extensively deployed in the scope of this thesis and requires a range of experimental setups. The pick-and-place process was carried out with major help from C. Pauly, group of xxx Mücklich, Saarland University. The nanomanipulator setup was provided by the same group.

1.1.1 Nanomanipulator

In general, nanomanipulator is a tip mounted inside an SEM, allowing manipulation and visualization of the manipulation process at the same time. The one used for our experiments was built by the company Kleindiek (model MM3A-EM) and has a changeable tungsten tip (see Figure 1.1b). It is mounted inside a Thermo Scientific™ Helios NanoLab™ DualBeam™ microscope, which combines a focussed ion beam and an electron microscope. The bent nanomanipulator tip has 3 degrees of freedom: up/down and left/right both in an arc up to 240° and 12 mm in/out (see arrows in Figure 1.1b). Before nanomanipulation the tip was "sharpened" with the focussed ion beam by etching away tungsten with gallium ions. This sharpening was performed to meet the size criteria necessary to pick up the nanodiamonds. In Figure 1.3a the sharpened tip is shown (the radius of curvature amounts to 100 nm). The small tip sticking out of the bigger cone is the sharp tip used for pick-and-place.

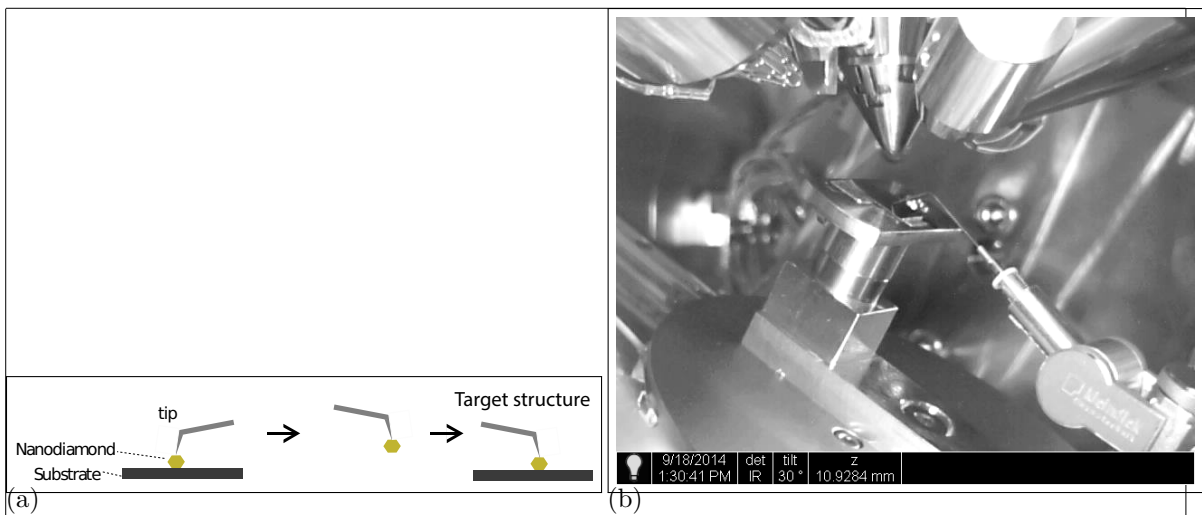


Figure 1.1: (a) Sketch of the pick-and-place process exploiting a nanomanipulator. (b) Image of the nanomanipulator mounted in the FIB. The arrows indicate the degrees of freedom of motion of the nanomanipulator. The custom made workbench is situated in the middle of the picture. On top of it, there is a 1cm^2 substrate with coated nanodiamonds, the nanomanipulator tip pointing to the middle of it. Behind it, there is the target vertical-cavity surface emitting laser. Perpendicular to the workbench, the objective of the electron microscope can be seen. The pointier cone perpendicular to the image top image edge is the objective of the focussed ion beam.

1.1.2 Determination of The Position of Nanodiamonds

An nanodiamond pre-characterized in the confocal setup exhibiting the preferred spectroscopic properties has to be found again in the SEM setup where the nanomanipulator is installed. Therefore, we milled cross markers into the iridium coating of the silicon substrate using the focussed ion beam prior to spin-coating the substrate with nanodiamond solution. The crosses' size is $10 \times 10 \mu\text{m}^2$ are exhibit a nominal depth of 40 nm. Four crosses are the cornerpoints of a $50 \times 50 \mu\text{m}^2$ square. The 10×10 crosses spaned one field of crosses; we usually put 3 fields of crosses on one substrate.

To record the position of a nanodiamond with respect to a cross marker, we used two different methods:

- Scanning the sample in the confocal setup while a white light source illuminates the sample from the side in an acute angle. The edges of the cross markers are visible in the fluorescence scan. After turning the white light lamp off, the same area is scanned once more to record the fluorescence from the SiV centers. An overlay of the two images identifies the position of fluorescent SiV centers with respect to the cross markers. The disadvantage of this method is, that it takes a lot of time, as every scan has to be performed twice. Also, as only fluorescence light scans are performed, no information of the nanodiamonds is accessible. Such information comprises of the size of the individual nanodiamonds and whether the nanodiamonds lie isolated on the substrate surface. These parameters are only available during the pick-and-place process in the SEM. An emitter with optimal optical properties can turn out not to be suited for pick-and-place just before the process itself, hence the time spent to optically characterize an emitter

fib pa-
rameter

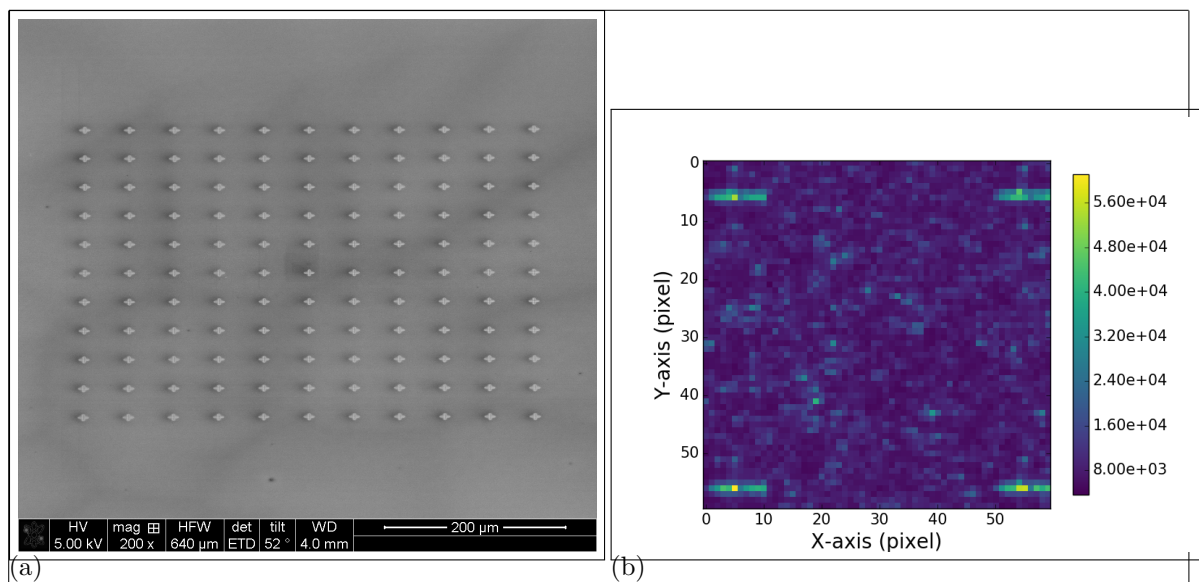


Figure 1.2: (a) Overview of a field of cross markers. The field spans 0.5×0.5 mm (b) White light scan of an area with a cross marker in all four corners.

was in vain.

- A more efficient method is scanning the substrate first in a commercial laser scanning microscope . The laser scanning microscope is a confocal microscope where the focus of a laser is used to obtain the height of a structure. It is possible to scan a whole field of cross markers in several minutes. The obtained image is a greyscale image, where the greyscale corresponds to the height deviation of a structure. Therefore, both the crosses and the nanodiamonds appear in darker shades of grey. So in contrast to the previous method, information on the size and isolation of the nanodiamonds is accessible. After scanning the substrate with the laser scanning microscope, it is put into the confocal setup. While observing the surface with the CCD camera (Figure 1.17), a specific cross marker is chosen as the starting point of a fluorescence light scan. Comparing the laser scanning microscope image and a fluorescence light scan, fluorescent dots of the fluorescence light scan are attributed to nanodiamonds in the laser scanning microscope scan (see Figures 1.12a and 1.12b).

specs
verify
info

1.1.3 The Pick-And-Place Process

After we identified nanodiamonds as well-suited for transfer to the target structure, both the substrate with the nanodiamonds and the target structure were mounted inside the SEM. The process was performed using a high resolution mode with a low acceleration voltage of the SEM of 1 keV and a current of 1.7 nA. The tip is approached to the pre-selected nanodiamond from above. As the SEM objective is mounted above the nanomanipulator, the proximity the nanomanipulator tip to the nanodiamond is not observable. The proximity is indirectly estimated by the shadow the tip casts onto the substrate and the focus. The first method is used for the coarse approachment of the tip to the nanodiamond: The closer the tip gets to the nanodiamond, the closer the shadow of the tip coincides with the nanodia-

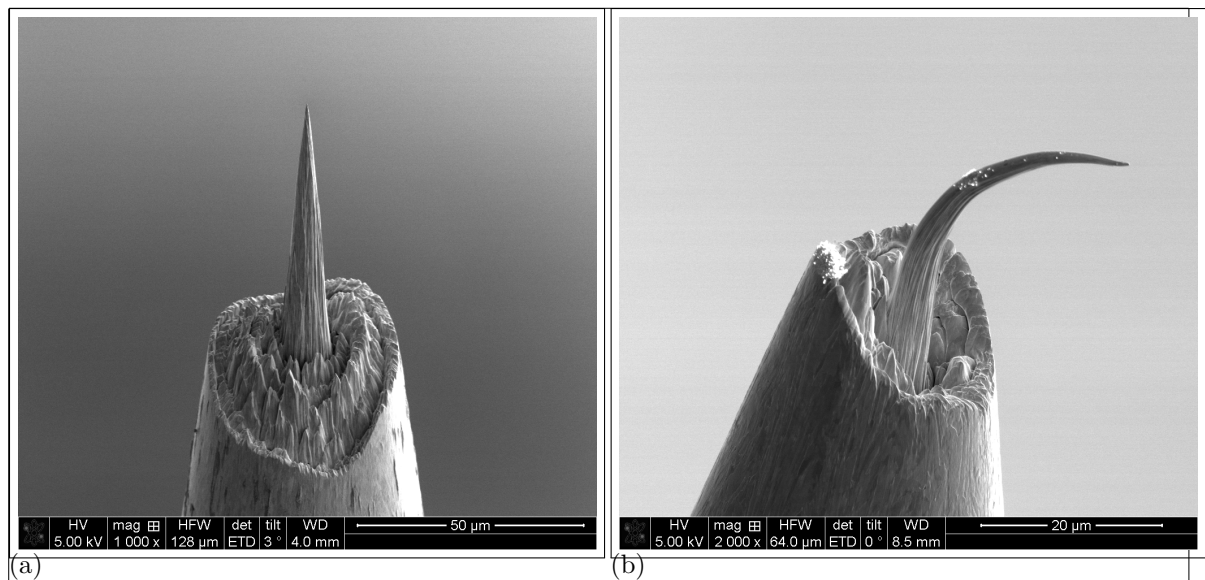


Figure 1.3

mond position. Exploiting the focus as an estimate for the proximity of the tip is used for fine adjustment during the last stage of the approachment. This is done as follows: At the end of the coarse movement, the tip of the nanomanipulator is still some distance above the nanodiamond. The SEM is focused on the nanodiamond, therefore the nanomanipulator tip is out of focus and appears blurry. As the tip is approached, it moves further and further into focus, its image becoming sharper, until the it touches the nanodiamond. As this is a tricky process, sometimes the tip was approached with too much force and was destroyed in the process (Figure 1.3b).

When performed correctly, due to adhesion, the nanodiamond sticks to the nanomanipulator tip when the both get in contact (Figure 1.15a). The nanomanipulator is then moved to the target structure and the same approachment procedure is applied. Dependent on the material of the target structure, the nanodiamond either sticks to the structure right away due to higher adhesion forces between the nanodiamond and the structure (as is the case for the golden plasmonic antennas). Or the nanodiamond has to be "wiped off" of the nanomanipulator tip in a sideways motion. In either way it is possible to place the nanodiamond within a precision of a few nanometers.

1.2 Coupling SiV centers to Vertical-Cavity Surface Emitting Lasers

For metrology, the photon flux rate has to be high enough to be measured by a low optical flux detector [1].

The red AlGaInP-based oxide-confined vertical-cavity surface emitting lasers (VCSEL) are compact and perfect candidates for excitation of SiV centers in a hybrid integrated single photon source: They exhibit wavelengths around 650 nm at continuous wave emission. SiV centers exhibit intensity maxima at an excitation at 670 nm and 690 nm [1]. In addition, VCSELs

diagram
einfuegen

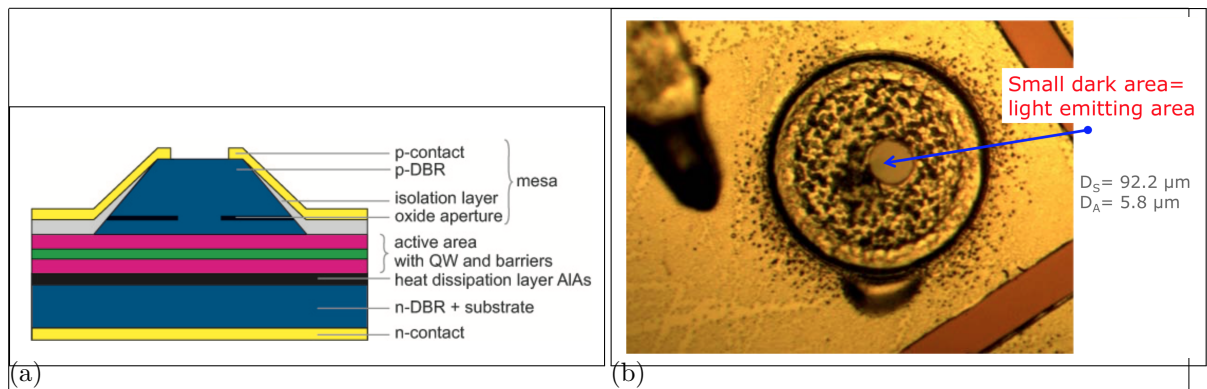


Figure 1.4: (a) Sketch of the VCSEL showing the different layers.

ask how to cite

(b) Image of the VCSEL. The circle with the black dots is the hole in the p-contact (diameter D_s , the smaller darker area in the middle is the laser output area (diameter D_A)

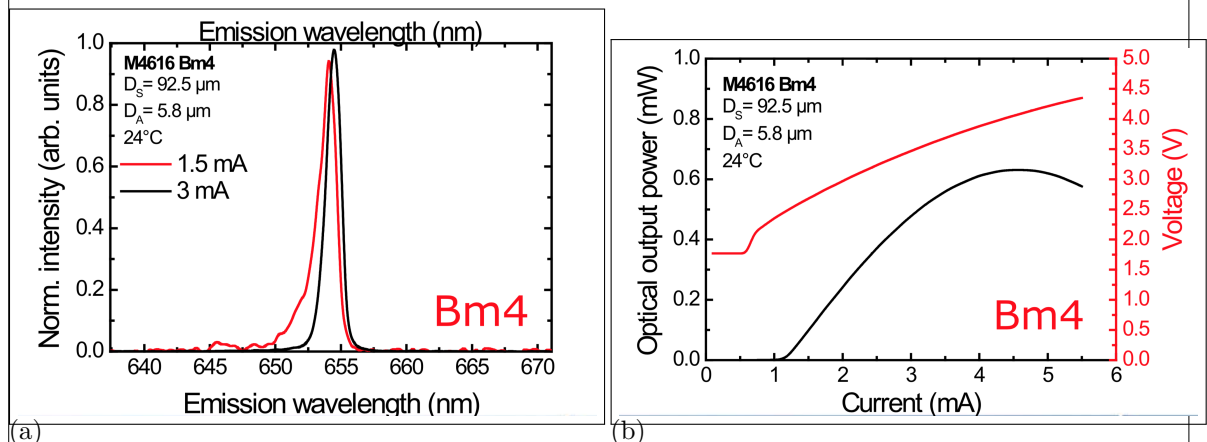


Figure 1.5: (a) Emission spectrum of the used VCSEL at two different currents. (b) Optical output power and voltage of the same VCSEL in dependence of input current. []

exhibit circular beam profile, have low divergence angle and emit linearly polarized light.

1.2.1 Vertical-Cavity Surface Emitting Laser Structure

The VCSEL structure (??) consists of an active region between two distributed Bragg reflectors (DBR). The bottom n-type DBR is made of 50 pairs of AlAs/Al_{0.5}Ga_{0.5}As, the p-type DBR consists of 36 Al_{0.95}Ga_{0.05}As/Al_{0.5}Ga_{0.5}As mirror pairs [2]. The active region consists of four GaInP quantum wells (QW). An oxide aperture in a field node of the standing wave serves as a spatial filter for maximum modal gain by confining the current and the optical mode. The active diameter which is defined by the oxide aperture amounts to 5.8 μm. As this region is the area where the laser emission exits the VCSEL, the nanodiamonds have to be put within this area. The used VCSEL exhibits an optical output power up to 1 mW with low threshold current of up to 3 mA at about 655 nm.

ist das
up to

nachdenken
wie for-
mulierung
richtig
ist

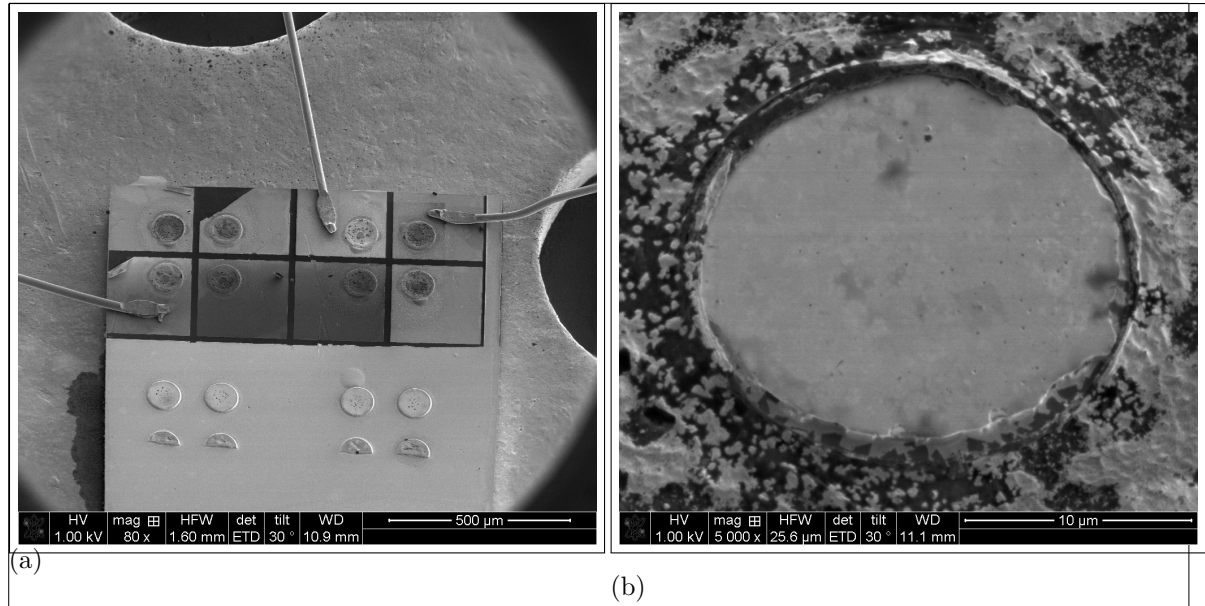


Figure 1.6: (a) SEM image of an array of VCSELs. The three wires are the anodes, which are connected to the top layer (p-contact) of the VCSEL. Therefore, three of the VCSEL structures can be operated. (b) Detail SEM image of the top of the exploited VCSEL Bm4. The circular middle part is the hole in the p-contact through which the top DBR is visible. The active diameter is smaller than that and not visible in the SEM.

1.2.2 SiV center in a Vertical-Cavity Surface Emitting Laser

As diamond material we used CVD grown nanodiamonds. They had been grown on an iridium coated silicon wafer (see ??). These nanodiamonds exhibit a nominal size of 200 nm. First, we selected a nanodiamond which exhibited one dominant line at 746.0 nm with a linewidth of 1.9 nm. Consecutively, its position on the substrate was determined using a white light laser scan as described in ?? . It was then transferred to the VCSEL Bm4 described in ?? . After a successful transfer of the pre-selected nanodiamond onto the active area of VCSEL Bm4, the VCSEL was put in the confocal setup. Using the laser from the confocal setup we checked if the pick-and-place process caused any modification of the spectroscopic properties of the SiV center such as a decrease of countrate or a modification of the fluorescence light spectrum. For this, the VCSEL itself was not operated itself. First, the VCSEL surface was scanned Figure 1.7a. A bright dot exhibiting a countrate of a few thousand counts per second is visible where the nanodiamond containing an SiV was put. A comparative scan of a VCSEL without nanodiamond only exhibits a background countrate, as expected (Figure 1.7b). The spectrum of the SiV center in the transferred nanodiamond was investigated before and after the pick-and-place process (Figure 1.8). The original spectrum before nanodiamond transfer exhibits a sharp line at 746.0 nm (denoted line A). After the pick-and-place process, this line is still there, albeit with a low intensity. Another line at 0 nm (denoted line B) which was a minor feature in the spectrum before pick-and-place, is the predominant line after the process. This modification of the spectrum is caused by a reduction of the intensity of line A and constant intensity of line B. The reduction of the intensity of line A may be caused by damage of the color center due to electron radiation. While the energy of the electrons is low compared to the ionization energy of the color center , we observed a reduction of fluorescence

was it
single?

check
number

numbers

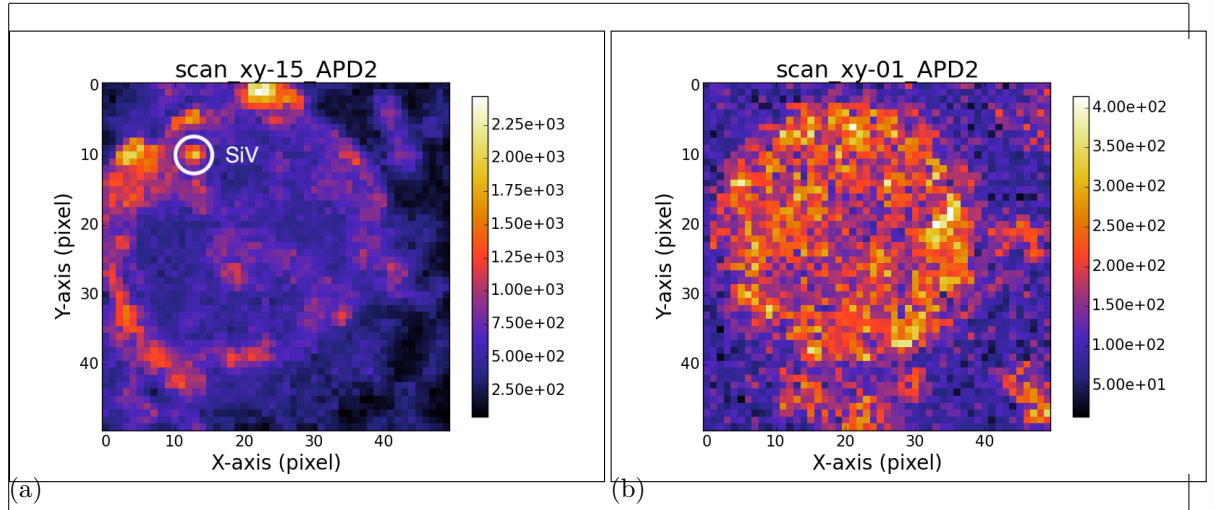


Figure 1.7: (a) Scan of the VCSEL Bm4 with coupled nanodiamond under excitation with the laser from the confocal setup. The big visible ring is the edge of the circular hole in the p-contact. The bright spot in the upper left corner corresponds to the transferred nanodiamond containing an SiV center. (b) Scan of the VCSEL Bm2 without nanodiamond under excitation with the laser from the confocal setup. The circular hole in the p-contact exhibits a constant count rate.

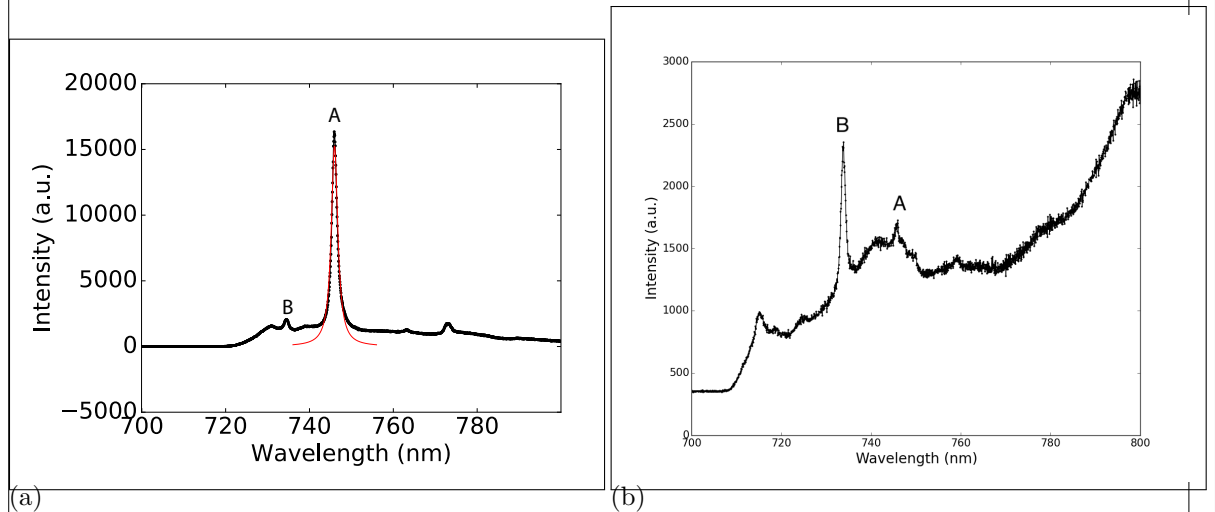


Figure 1.8: (a) Spectrum of the preselected diamond for transfer onto VCSEL Bm4 before pick-and-place. The strong line denoted A exhibits a center wavelength of 746.0 nm and a linewidth of 1.9 nm. Line B exhibits a center wavelength of 0 nm and a linewidth of 0 nm

put in correct numbers

(b) Spectrum of the same SiV center after pick-and-place, excited with the same laser as before. While Line A is almost gone, line B still exists and is the predominant line of the spectrum. Note: different longpass filters were used for the two measurements. Measurement (a) was performed with a 720 nm longpass filter, measurement (b) with a 710 nm longpass filter.

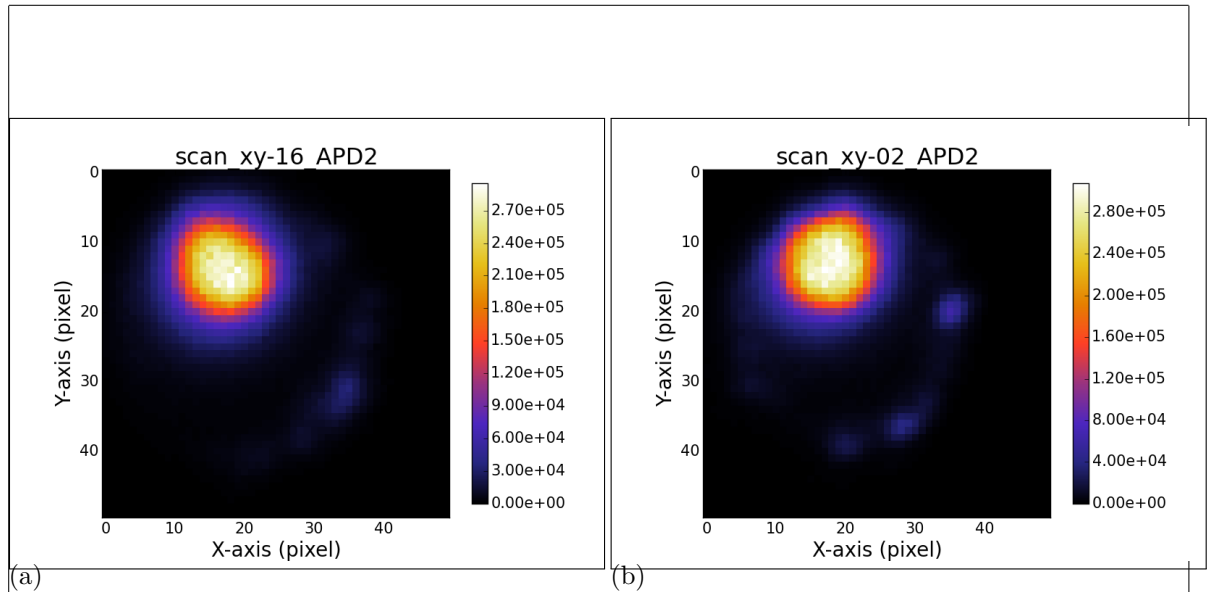


Figure 1.9: (a) Scan of the laser light stemming from the VCSEL Bm4 and the fluorescence light from the SiV center in the filter window 730 nm to 750 nm. (b) Scan of the laser light stemming from the VCSEL Bm2 without coupled SiV center. The outcome of the two scans is almost identical.

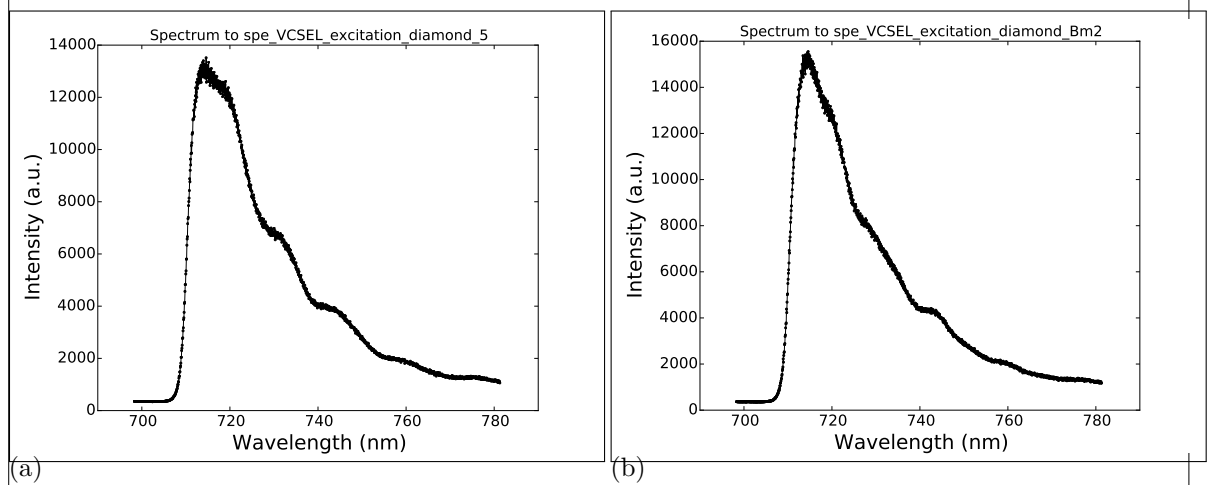


Figure 1.10: (a) Recorded Spectrum of the SiV center in the transferred nanodiamond on VCSEL Bm4 during VCSEL operation. No distinct SiV center lines are visible. (b) Recorded spectrum of VCSEL Bm2 (without SiV center)

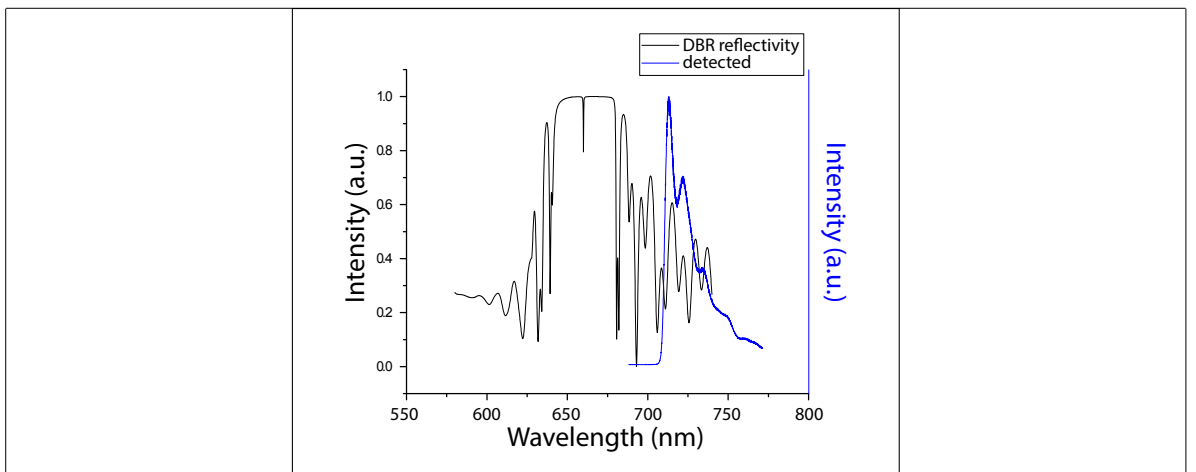


Figure 1.11: Reflectivity of the Distributed Bragg reflector (DBR) of the VCSEL, and spectrum of the SiV center measured during VCSEL excitation. The reflectivity of the DBR and the VCSEL emission spectra are depicted with different scales. The shape of the measurement of the SiV center during VCSEL operation coincides with the shape of the DBR reflectivity. The spectrum of the SiV center is not visible. As the emission from the SiV center is small compared to the intensity of the laser sideband in the same wavelength regime, the SiV centers emission is not detectable

warum schaut das spectrum anders aus als das, was einzeln geplottet ist?

light intensity after electron radiation (for a detailed description of this effect, refer to [?]). We then operated the VCSEL at 0.84 mA and 3.3 V and turned off the laser of the confocal setup. We scanned both the surface of VCSEL Bm4 (with nanodiamond) and of VCSEL Bm2 (without nanodiamond) with a 730 nm to 750 nm bandpass filter. This filter window suppresses the VCSEL laser line at 655 nm (1.5a) while leaving the SiV center emission nearly unchanged. The light areas in Figure 1.9 correspond to the laser output areas. We measured a spectrum at the same points as before VCSEL operation. In the case of VCSEL Bm4, this spot corresponds to the position of the SiV center. The following observations are made from the measurements:

- In both scans, the laser output area is visible as a big bright spot. There is no difference in intensity between VCSEL Bm4 and Bm2.
- The spectra of VCSEL Bm4 and Bm2 are almost identical.

The spectrum recorded in the confocal setup corresponds well with the DBR reflectivity (Figure 1.11). Hence, we conclude, that the detected emission is due to the VCSEL and does not stem from the SiV center. From these observations, we draw the conclusion that the fluorescence light emission from the SiV center is small compared to the sideband of the VCSEL emission in the wavelength regime where the SiV center emission is expected. Therefore, the SiV center emission is not detectable during VCSEL excitation.

Ongoing work is performed to reduce sideband emission of the VCSEL in the SiV center emission regime. A promising approach is to add a gold layer on top of the VCSEL which acts as a tunable mirror. While films of gold have a transmittance maximum at 500 nm, the

besser
begruen-
den, was
passiert

ev besser
begruen-
den

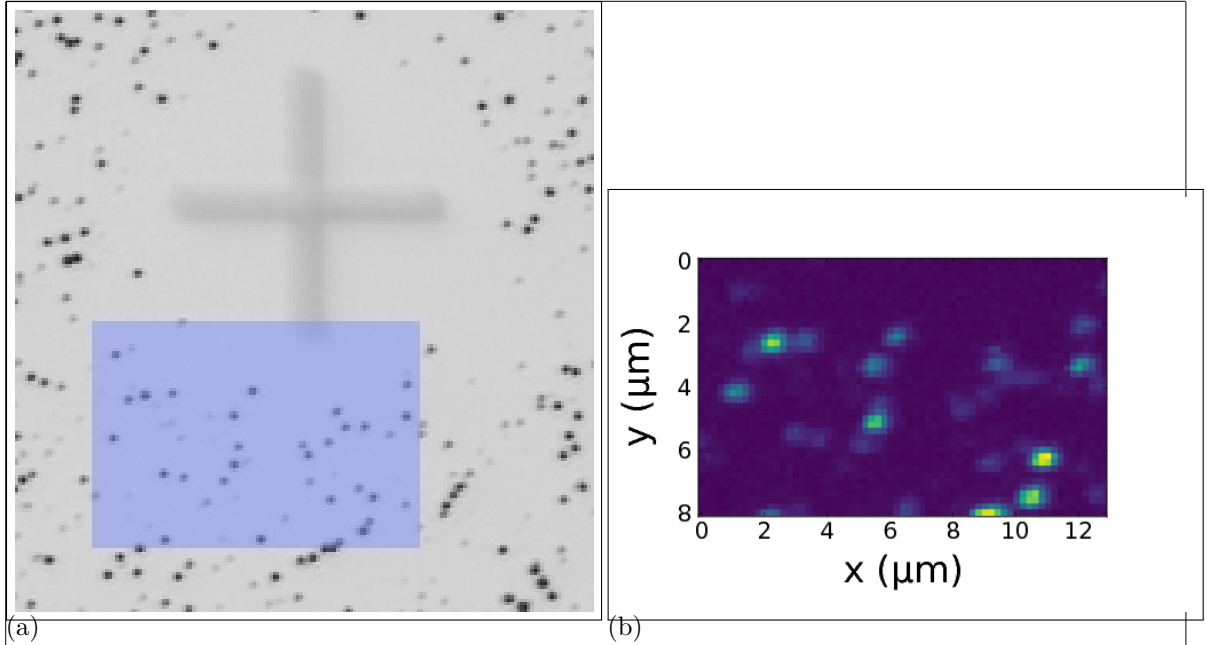


Figure 1.12: (a) Picture recorded with a commercial high resolution laser scanning microscope. The area shaded in blue represents the photoluminescence scan in image (b). (b) Photoluminescence scan of a $8 \mu\text{m} \times 13 \mu\text{m}$

transmittance minimum depends on the film's thickness [3]. Hence the goal is to apply a gold film which suppresses the laser sideband in the SiV center emission regime.

In this chapter we showed successful transfer of a nanodiamond containing an SiV center. While the SiV center spectrum was modified after the pick-and-place process, it was clearly identified with the preselected SiV center. Further research has to be performed to enhance the VCSEL emission properties.

1.3 Coupling Nanodiamonds to Double Bowtie Antenna Structures

In this chapter, the integration of SiV centers in nanodiamonds with double bowtie nanoantenna structures is presented. The emission from the coupled system has two advantages:

- The antenna causes an enhancement in the SiV center's photoluminescence emission intensity.
- The photoluminescence spectrum of the nanodiamond is modified depending on the geometry of the nanoantenna as well as the position of the emitter in the gap. This provides the flexibility of designing the nanoantennas to accurately predict and tune the emitters' PL spectrum as desired.

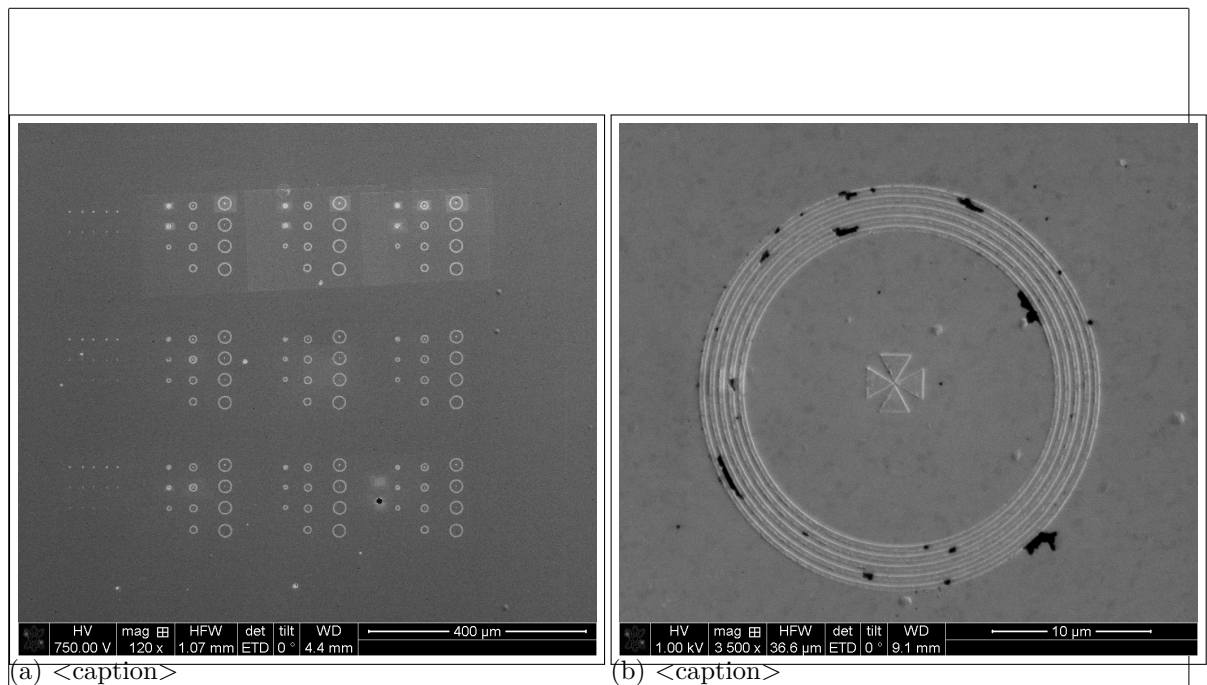


Figure 1.13: <caption>

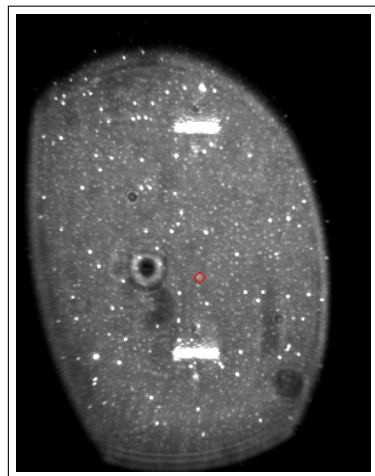


Figure 1.14: Image of the sample surface of 100 nm wet-milled nanodiamonds spin-coated on an iridium substrate illuminated with diffuse white light. The white bars are the horizontal bars of the cross markers which serve as a coarse orientation on the sample surface, the white dots are nanodiamonds, the big black spot is an artifact.

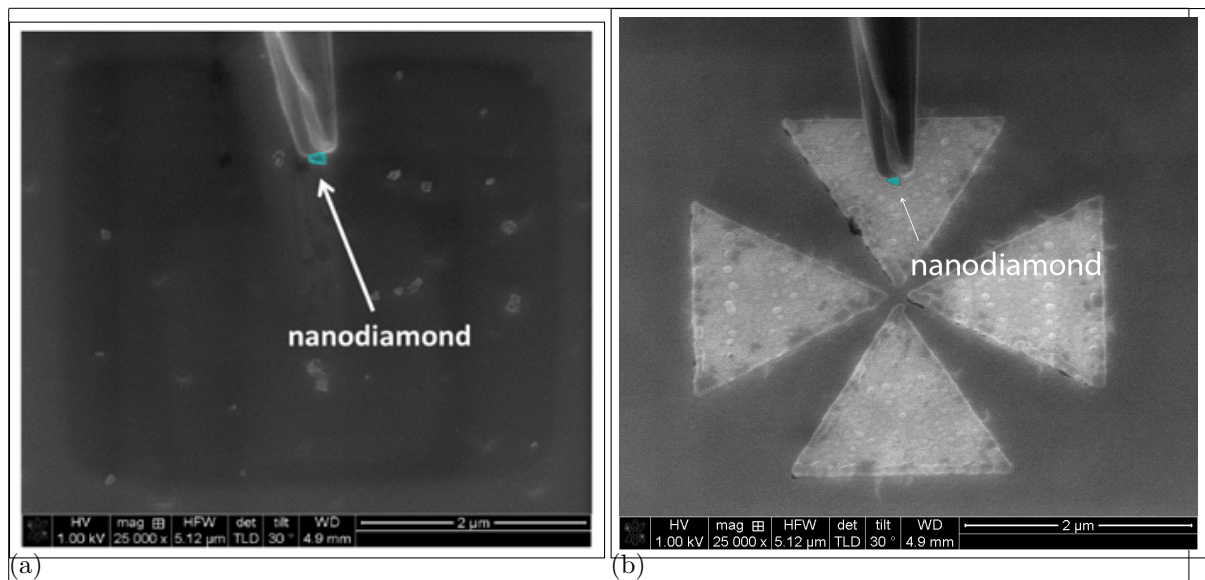


Figure 1.15

1.3.1 Plasmonic Antennas

[4] Optical antennas, acting as converters between propagating and localized fields, provide an effective route to couple photons in and out of nanoscale objects. These antennas are the counterparts of conventional radio and microwave antennas and operate in the visible regime (1, 2). Optical antennas have been shown to focus optical fields to subdiffraction-limited volumes (3), enhance the excitation and emission of quantum emitters (4 \AA), and modify their spectra (8).

A characteristic of antennas is their directed emission and reception. So far, the control of directionality has mainly been pursued by photonic crystal structures (9) and surface-plasmon-based devices (10–12). However, for such structures approaching the nanometer scale diffraction can limit the collimated beaming of light. On the other hand, the interaction of quantum emitters with light is best enhanced with microcavities (13, 14). Compared with these approaches, plasmonic nanoantennas offer a much smaller footprint in an open geometry combining strong subwavelength fields and increased transition rates, together with the prospect of directionality.

[5] from gold, a metal that can develop charge oscillations in its surface layers when excited by optical radiation. These antennas allow visible radiation, which has wavelengths of hundreds of nanometers, to couple into a semiconductor quantum dot only a few nanometers in diameter, and also direct the emission

Good mode-matched antennas reradiate their energy after excitation within a single cycle of the wave. Molecules or quantum dots take nanoseconds or even longer to reradiate their energy. This time scale corresponds to about 1 million oscillations at optical frequencies, and the emission is in all directions.

If an atom, molecule, or quantum dot is placed into the near-field of a metallic nanoantenna (within about 1/50th the wavelength of the emitted radiation), its excited state can radiate photons very efficiently to free space (see the figure, panel B). The quantum emitters can emit a single photon, which can be exploited in quantum optics. Additionally, the

nanoantenna can redirect radiation into a defined solid angle in space and impose a specific polarization on it.

The demonstration of the Purcell effect, which is the acceleration of the decay of the quantum emitter caused by impedance matching by the antenna to free space, could also enhance the radiative emission over nonradiative losses

[6] The electro-magnetic antenna, originally referred to as an "aerial", is a transducer between electromagnetic waves and electric currents, and generally operates in the radiofrequency regime. In analogy with the electro-magnetic antenna, we define the optical antenna as a device that converts freely propagating optical radiation into localized energy, and vice versa. The spatial extent of a receiver or transducer is commonly much smaller than the wavelength of radiation, λ , and is typically of the order of $\lambda/100$.

Surface plasmon resonances make optical antennas particularly efficient at selected frequencies. A generic antenna problem is illustrated in Fig. 3. It consists of a transmitter and a receiver, both represented by dipoles p . The antenna is introduced to enhance the transmission efficiency from the transmitter to the receiver. This enhancement can be achieved by increasing the total amount of radiation released by the transmitter, for which the antenna efficiency is a useful figure of merit:

$$\eta = \frac{P_{rad}}{P_{loss}} \quad (1.1)$$

where P is the total power dissipated by the antenna, P_{rad} is the radiated power and P_{loss} is the power dissipated through other means, such as by absorption in the antenna. However, the transmission efficiency can also be improved by directing the radiation in the direction of the receiver. The efficiency for this process is represented by the directivity:

$$\eta = D \quad (1.2)$$

where the angles $\hat{\theta}$ and $\hat{\phi}$ represent the direction of observation and $D(\hat{\theta}, \hat{\phi})$ is the angular power density. The combination of antenna efficiency and directivity is referred to as the antenna gain:

$$G = \eta D \quad (1.3)$$

By reciprocity, we can interchange the fields and sources in Fig. 3 to give $G = \eta D$, where E_1 (E_2) is the field of dipole p_1 (p_2) evaluated at the location of p_2 (p_1). A good transmitting antenna is therefore also a good receiving antenna. For a transmitter in the form of a two-state quantum emitter, reciprocity leads to a relationship between the emitter's excitation rate \dot{N}_{exc} and its spontaneous emission rate:

$$\eta = \frac{\dot{N}_{exc}}{\dot{N}_{em}} \quad (1.4)$$

Here, the superscript "0" refers to the absence of the antenna and the subscript "1" indicates the polarization state; that is, the electric field vector points in the direction of the $\hat{\theta}$ unit vector. An equivalent equation holds for polarization in the $\hat{\phi}$ direction. Interestingly, excitation in a direction of high directivity allows the excitation rate to be enhanced more strongly than the radiative rate. Another important antenna parameter is the antenna aperture, which is formally the same as the absorption cross-section sigma. Let us consider a dipole-like receiver with a cross-section σ that is not coupled to an antenna. The unit vector in the direction of the absorption dipole axis is denoted as n_p and the incident field at the location of the receiver is E_0 . Once we couple the receiver to an antenna, the field at the receiver increases to E and the cross-section or antenna aperture becomes

$$\eta = \frac{\sigma}{\sigma_0} \quad (1.5)$$

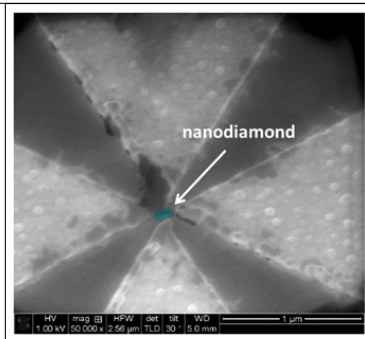


Figure 1.16: <caption>

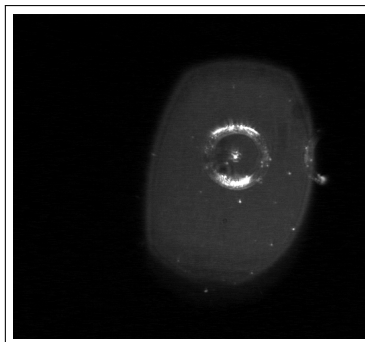


Figure 1.17

Thus, the aperture of an optical antenna scales with the local intensity enhancement factor. Theoretical and experimental studies have shown that intensity enhancements of 10^4 – 10^6 are readily achievable^{14,36,37} and hence, for typical molecules with π -free-space cross-sections of $\sigma_{\text{mole}} = 1 \text{ nm}^2$, we find that a layer of molecules spaced $0.1\text{--}1 \text{ nm}$ apart can absorb all of the incident radiation if each molecule is coupled to an optical antenna. Of course, this estimate ignores the coupling between antennas and therefore has limited validity.

1.3.2 Structure of the Plasmonic Antennas

FDTD numerical simulations were performed using Lumerical software to characterize gold double bowtie nanoantennas on a gold substrate. The nanoantennas are tailored to have a gap of $g = 150 \text{ nm}$ (taking into account the diameter of the nanodiamonds of around 100 nm), side length of $L = 2 \mu\text{m}$, and a thickness of $t = 60 \text{ nm}$ (see Fig. 3a). Upon excitation with incident light, an intense electromagnetic hotspot is formed in the nanoantenna gap [7], which is expected to excite a nanodiamond containing SIV centers aiming to enhance its fluorescence emission. Unlike a single bowtie that is sensitive only to the polarization along its principle axis (C₂ rotational symmetry), a double bowtie features a C₄ rotational symmetry and therefore focuses both parallel and perpendicular polarizations (i.e. all in-plane directions). The index of refraction of gold is taken from Palik [8], and that of the nanodiamond is chosen to be $n = 2.4$ at $\lambda = 660 \text{ nm}$. The electric field intensity in the nanoantenna gap is then measured as a function of wavelength to identify the antenna resonance. The spectrum is given in Fig. 3b where we observe that the resonance shows two peaks; an intense peak coinciding with the

read paper

Palik, E. D. Handbook of optical constants of solids. 3, (Academic press, 1998)

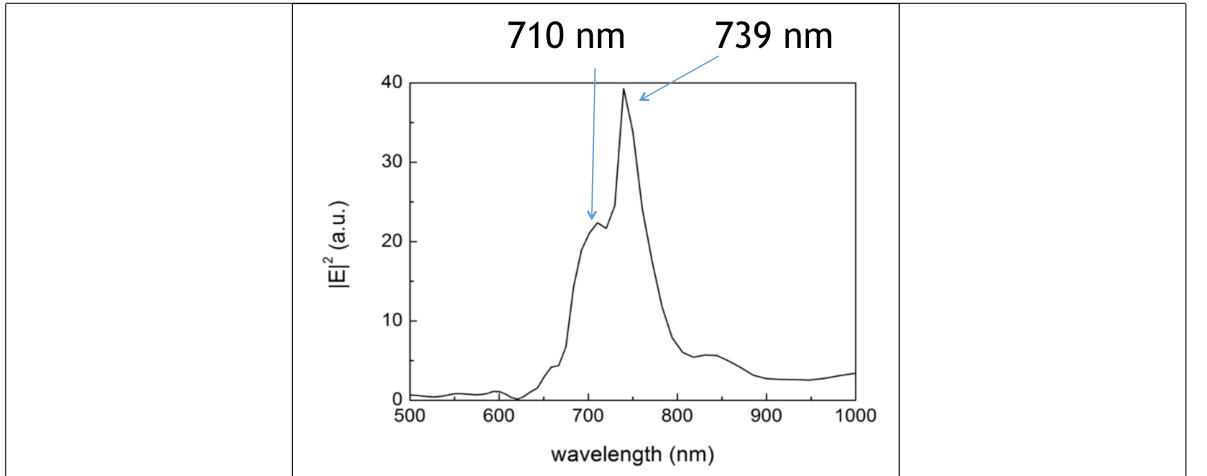


Figure 1.18: <caption>

SiV emission wavelength ($\lambda = 739 \text{ nm}$), and an additional mode at a lower wavelength ($\lambda = 710 \text{ nm}$) [8]. The resonance spectrum of the antenna alone shows only one peak at 739 nm. Thus, the additional peak is attributed to the presence of the nanodiamond that is slightly shifted from the center of the gap, corresponding to our experimental conditions. These calculations suggest, that the emission from an SiV center at 738 nm is effectively enhanced and directed by the antenna.

1.3.3 SiV center in a Plasmonic Double Bowtie Antenna

In the following, specific details and challenges concerning the coupling process are given and results of the spectroscopic measurements of an SiV center in a plasmonic double bowtie antenna are reported.

We performed coupling the nanodiamonds containing SiV centers in two approaches: First we chose a nanodiamond containing several SiV centers for pick-and-place and afterwards a nanodiamond containing a single SiV center. As mentioned before, single SiV centers may be damaged by the electron radiation in the SEM during pick-and-place and stop emitting photoluminescence light. Hence, we decided to run first experiments with nanodiamonds containing multiple SiV centers. This approach has the advantages that we are able to gain experience in the execution of the pick-and-place process without the risk of permanently damaging the emitter and therefore rendering the tedious pick-and-place process futile. For measurements of the intensity enhancement by the antenna, a single emitter is necessary. However, the antenna's influence on the SiV center spectrum can be studied when several emitters are present. Therefore, studies of the spectrum are performed in this first approach.

After we gained experience with the first approach, we searched for a suited nanodiamond containing a single SiV center. The aim was to perform saturation and second order correlation measurements to probe single SiV centers, and consequently quantify the exact Purcell enhancement imposed by the nanoantenna on a single photon emitter.

Nanodiamond With Multiple SiV centers Coupled to Antenna

The nanodiamonds exploited for the approach of coupling multiple SiV centers to an antenna were produced by a wet-milling process from a CVD diamond film¹. The solution of nanodiamonds which exhibit a median size of 100 nm were spin-coated on an iridium substrate treated with Piranha etch. To ensure that a pre-characterized nanodiamond exhibiting preferred optical properties (eg. narrow linewidth, high count rate) is later found again, the iridium substrate was engraved with reference cross markers produced by a focused ion beam prior to the spin-coating process. After spin-coating, the sample was placed in an oven for 3 hours at 450 °C to oxidize the surface and remove any residual graphite and amorphous carbon.

Figure 1.21a shows the spectrum recorded of the preselected nanodiamond. The ZPL peak exhibits a wavelength of 738.55(1) nm and a linewidth of 5.00(3) nm. These numbers correspond well to the ZPL of unstrained SiV centers and therefore allows us to deduce that the studied nanodiamond contains at least one SiV center. Photon autocorrelation measurements revealed, that the nanodiamond contains multiple SiV centers.

To determine the position of the nanodiamond on the original substrate, first a scan with a commercial laser scanning microscope (LSM) was performed as described in ?? . Figure 1.12a shows a part of an obtained LSM image. The cross marker can easily be identified, the black dots are nanodiamonds. After transferring the sample into the confocal setup, confocal scans of the corresponding areas are performed (Figure 1.12b). The area corresponding to the fluorescence light scan in Figure 1.12b is shaded blue in Figure 1.12a. When looking closely, the bright spots in the fluorescence light scan can be identified with nanodiamonds visible in Figure 1.12a. The image in the SEM is very similar to the image obtained by the LSM. Therefore, once a nanodiamond containing a preselected emitter is identified in the LSM scan, it is easy to find the same emitter in the SEM.

The picking part of the pick-and-place process was performed in the same manner as described in the section about VCSELs (??). The gold surface of the plasmonic antenna caused a high adhesion between the antenna surface and the nanodiamond. Once the nanodiamond touched the gold, it could not be picked up again with the tungsten tip. The nanodiamond first touched the antenna structure a few nanometers away from the gap and immediately stucked to the surface, on top of one of the triangles. Therefore, the nanodiamond had to be pushed into the gap with the nanomanipulator tip. This process caused some damage to the antenna structure. The damage is visible as black area at the tip of the top triangle in Figure 1.16. However, FDTD simulations of damaged antennas reveal that this modification of the antenna hardly influences the antenna resonance.

After this deterministic placement we measure the PL spectrum of the nanodiamond to identify the effect of the nanoantenna on its emission. The result is displayed in Figure 1.21a. The additional peak at a lower wavelength is attributed to the antenna resonance mode. To verify this, we convolute the experimental PL spectrum of the nanodiamond measured before placing it in the nanoantenna (Figure 1.20b) with the intensity spectrum of the nanoantenna obtained by simulations (Figure 1.18). The resulting spectrum is given in Figure 1.21b, and is in good agreement with the measured spectrum in Figure 1.21a, confirming that indeed the extra peak is due to the antenna resonance.

¹wet-milling performed by A. Muzha, group of A. Krueger, Julius-Maximilians Universität Würzburg, diamond film grown by group of O. Williams, School of Engineering, Cardiff University

fehlergrenzen
verfünen
machen

bild dazu

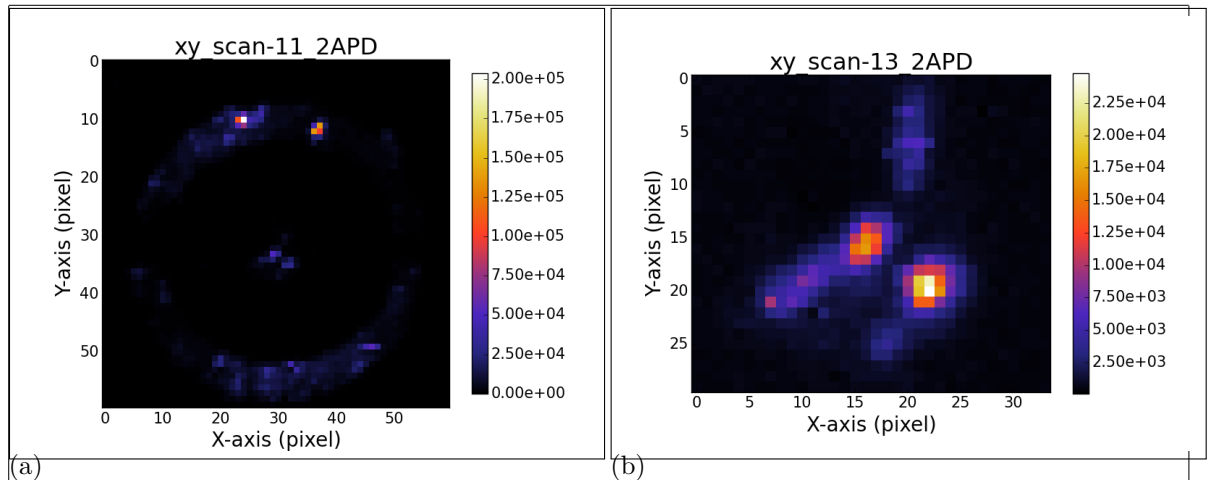


Figure 1.19: <caption>

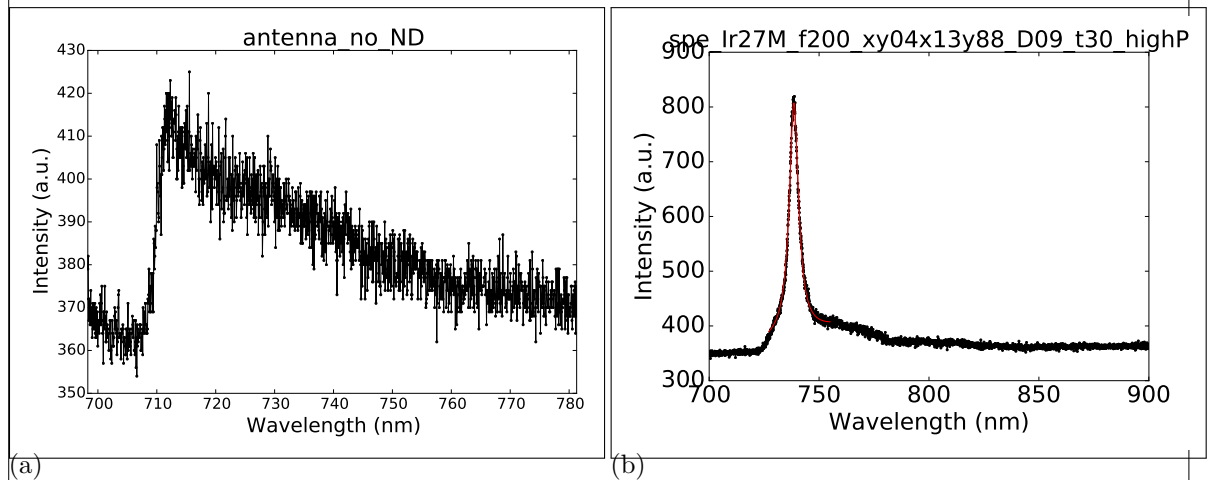


Figure 1.20: <caption>

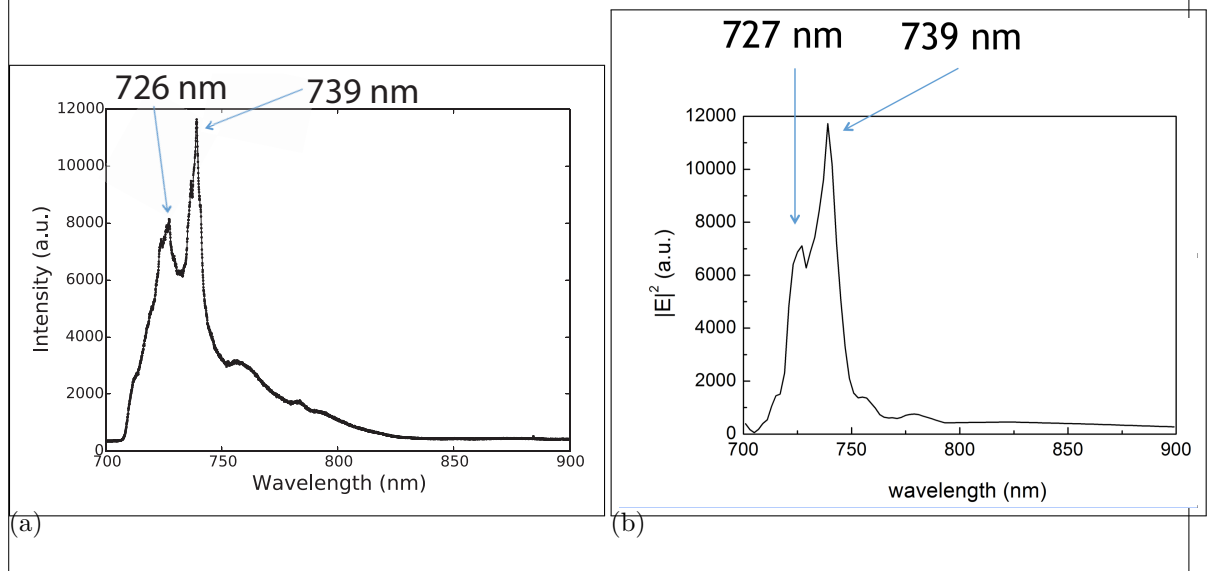


Figure 1.21: <caption>

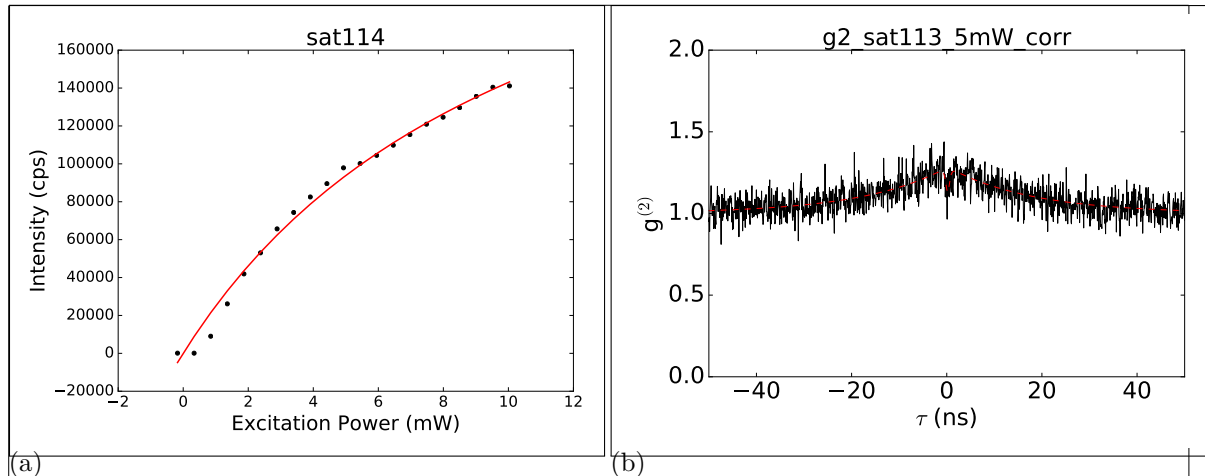


Figure 1.22: <caption>

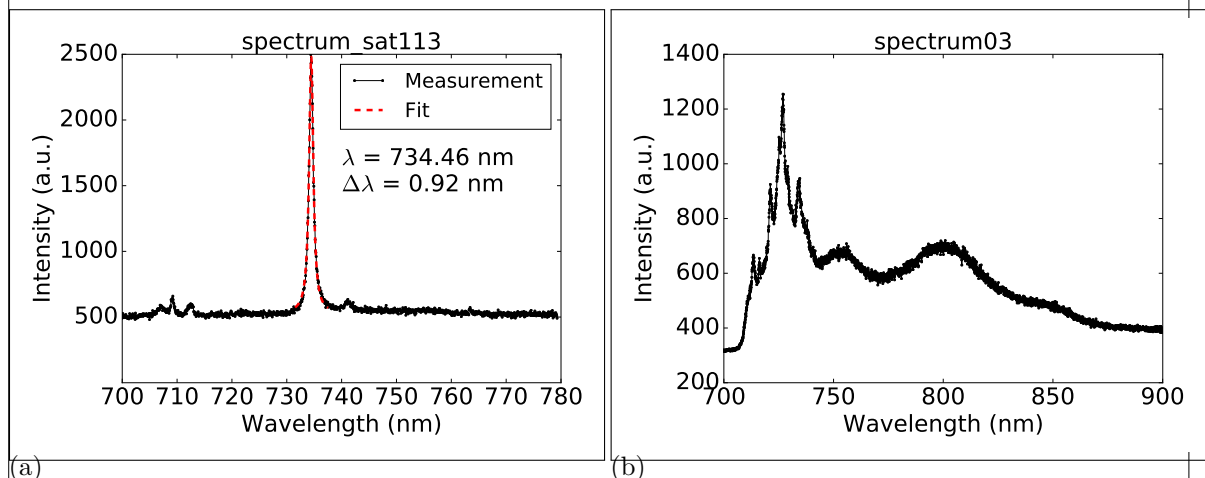


Figure 1.23: <caption>

Nanodiamond With Single SiV center Coupled to Antenna

sample M02-16: drop-casted with SiGH45 First, only a small percentage of the technically suited nanodiamonds (size, isolation) contain a single SiV center, second, damage due to electron radiation during pick-and-place. After an SiV center with a small dip in the $g^{(2)}$ function, indicating only few SiV centers.

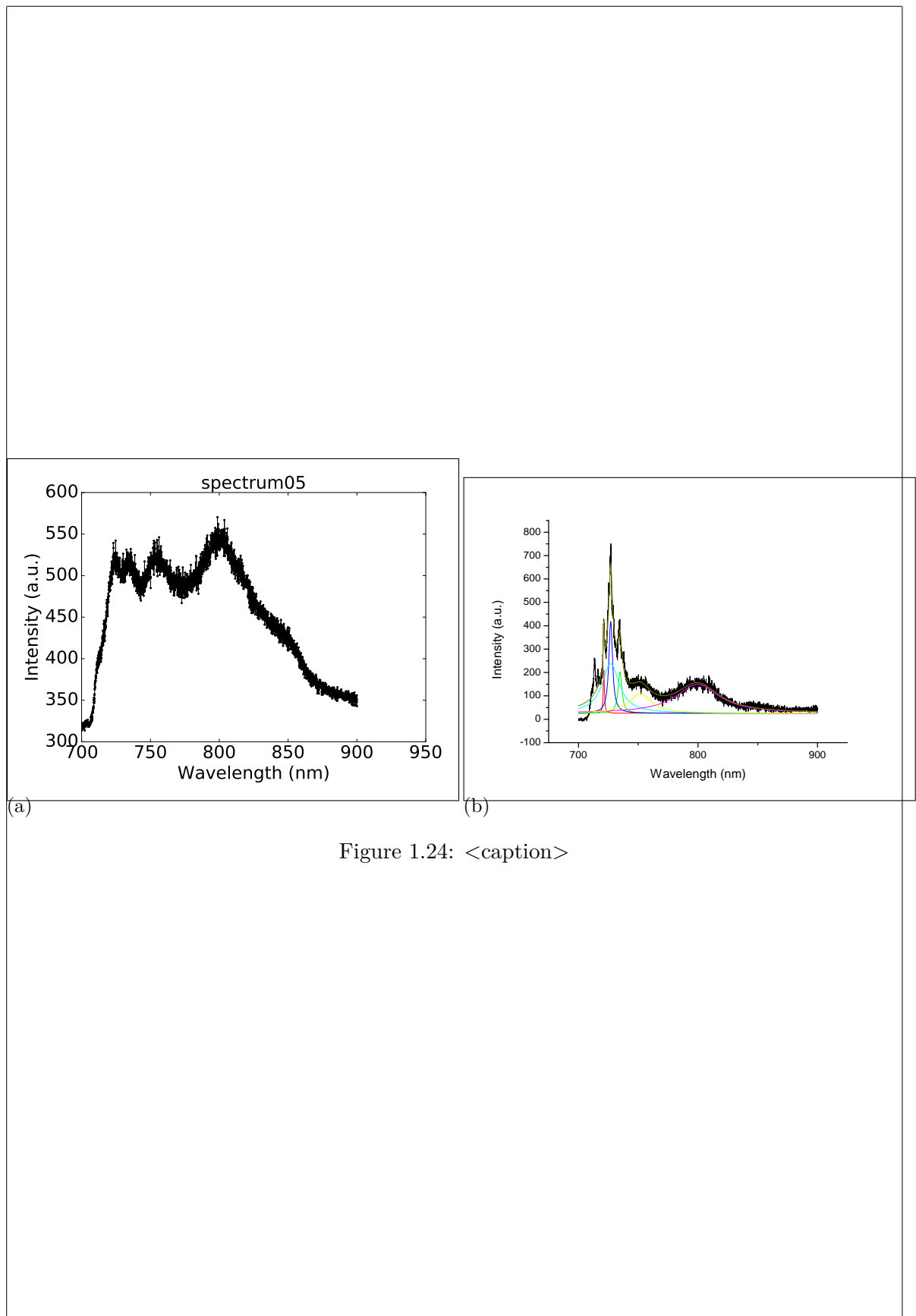


Figure 1.24: <caption>

Bibliography

- [1] Aigar Vaigu, Geiland Porrovecchio, Xiao Liu Chu, Sarah Lindner, Marek Smid, Albert Manninen, Christoph Becher, Vahid Sandoghdar, Stephan Götzinger, and Erkki Ikonen. Experimental demonstration of a predictable single photon source with variable photon flux. *Metrologia*, 54(2):218–223, 2017. 1, 5
- [2] Susanne Weidenfeld, Hendrik Niederbracht, Marcus Eichfelder, Michael Jetter, and Peter Michler. Transverse mode and polarization characteristics of AlGaInP-based VCSELs with integrated multiple oxide apertures. In Krassimir Panajotov, Marc Sciamanna, Angel Valle, and Rainer Michalzik, editors, *Proc. SPIE*, volume 8432, page 843205, jun 2012. 6
- [3] A. Axelevitch, B. Gorenstein, and G. Golan. Investigation of Optical Transmission in Thin Metal Films. *Physics Procedia*, 32(April 2016):1–13, 2012. 11
- [4] Alberto G Curto, Giorgio Volpe, Tim H Taminiau, Mark P Kreuzer, Romain Quidant, and Niek F van Hulst. Unidirectional emission of a quantum dot coupled to a nanoantenna. *Science (New York, N.Y.)*, 329(5994):930–933, aug 2010. 13
- [5] Harald Giessen and Markus Lippitz. Physics. Directing light emission from quantum dots. *Science*, 329(5994):910–911, aug 2010. 13
- [6] Lukas Novotny and Niek van Hulst. Antennas for light. *Nature Photonics*, 5(2):83–90, feb 2011. 14
- [7] N. Rahbany, W. Geng, S. Blaize, R. Salas-Montiel, R. Bachelot, and C. Couteau. Integrated plasmonic double bowtie / ring grating structure for enhanced electric field confinement. *Nanospectroscopy*, 1(1):61–66, 2015. 15
- [8] Nancy Rahbany. Towards integrated optics at the nanoscale : plasmon-emitter coupling using plasmonic structures. 2016. 16